Supplemental Information

October 16, 2015

Dynamic force quadratures

We have previously introduced a method [1] based on Intermodulation AFM (ImAFM) [2, 3] to rapidly measure the amplitude dependence of the tip-surface force quadratures at each pixel of an image while scanning at normal speed for dynamic AFM (1 line per second, 256 pixels per line). Here we recapitulate the basic ideas behind the force quadratures.

A cantilever freely oscillating far from a surface has a linear dynamics which is most easily described in the frequency domain,

$$\hat{d}(\omega) = \hat{\chi}(\omega)\hat{F}(\omega). \tag{S1}$$

The hat denotes a frequency-dependent complex number, so that Eq. (S1) is actually two linear equations relating the Fourier cosine (real) and sine (imaginary) coefficients of the deflection $\hat{d}$ and the force $\hat{F}$ at each frequency ω. For micro-cantilevers operating in air or vacuum, the linear response function $\hat{\chi}(\omega)$ of each eigenmode has the form of a simple harmonic oscillator,

$$\hat{\chi}(\omega) = \frac{1}{k}\left(1 - \frac{\omega^2}{\omega_0^2} + i\frac{\omega}{\omega_0 Q}\right)^{-1} \tag{S2}$$

where $\omega_0 = \sqrt{\frac{k}{m}}$ and $Q = \frac{\omega_0}{\gamma}$ are the resonance frequency and quality factor, related to the modal mass m, stiffness k and half-width of the resonance γ.

For the fundamental bending eigenmode there exists a good method to calibrate the three constants describing the response function [4, 5, 6]. One can then determine tip surface force by monitoring the steady-state response of the eigenmode to the total external force,

$$F(t) = F_{\mathrm{TS}}(t) + F_{\mathrm{D}}(t) \tag{S3}$$

where $F_{\mathrm{D}}(t)$ is a periodic driving force. Eq.(S1) can be solved for the Fourier coefficients of the tip-surface force,

$$\hat{F}_{\mathrm{TS}} = \hat{\chi}^{-1}(\hat{d} - \hat{d}_{\mathrm{free}}) \tag{S4}$$

where the free response spectrum $\hat{d}_{\mathrm{free}} = \hat{\chi}\hat{F}_{\mathrm{D}}$ is measured by retracting the probe well away from the surface where $F_{\mathrm{TS}} = 0$. Thus we determine the tip-surface force, separating it from the inertial and damping force associated with the motion of the cantilever body.

A stiff cantilever oscillating in air has a high quality factor resonance and $\hat{\chi}(\omega)$ is sharply peaked near $\omega = \omega_0$. High Q means that the cantilever response is greatly enhanced for Fourier components of the tip-surface force near the resonant frequency. Measuring this response as a dense frequency comb with spacing $\Delta\omega << \omega_0$ enables a description of the motion with two well separated time scales: a fast time scale corresponding to period of cantilever oscillation $T = 2\pi/\omega_0$, and a slow time scale corresponding to the period of the entire motion $T_m = 2\pi/\Delta\omega$. For each fast period, with nearly constant amplitude A, we extract the force quadratures which are Fourier coefficients of the tip-surface force, or integrals of the tip-surface force over a single oscillation cycle where the *tip motion has zero phase*[1].

$$F_I = \frac{1}{T}\int_0^T F_{\mathrm{TS}}(t)\cos(\omega_0 t)dt \tag{S5}$$

$$F_Q = \frac{1}{T}\int_0^T F_{\mathrm{TS}}(t)\sin(\omega_0 t)dt \tag{S6}$$

$$z(t) = h + A\cos(\omega_0 t) \tag{S7}$$

In the frequency domain we write,

$$\hat{F}_{\mathrm{TS}}(\omega_0) = F_I(A) + iF_Q(A) \tag{S8}$$

$$\hat{d}(\omega_0) = A + i0. \tag{S9}$$

From the measured motion we can calculate the phase rotation required to enforce Eq. S9. Applying this rotation to the Fourier coefficients $\hat{F}_{\mathrm{TS}}(\omega_0)$ determined from Eq. S4, we get the force quadratures [7, 8, 9]. The method extracts two curves at each pixel, $F_I(A)$ and $F_Q(A)$. Here we note that the oscillation frequency in Eqs. S5-S7 is not necessarily the resonance frequency ω_0. However, to achieve large SNR at many frequencies in the response comb one is limited to a 'carrier frequency' close to resonance. A slight detuning of this carrier frequency results in an additional overall phase factor in the complex envelope functions of both force and motion. This phase factor disappears when the Force quadratures are defined with respect to the phase of the tip motion[9]. We also note that F_I is proportional to an instantaneous oscillation 'frequency shift' [7], an interpretation used in the context of Frequency Modulation AFM (FM-AFM) [10] where frequency shift is measured with a phase-locked-loop.

Moving surface model

Consider the tip oscillating in close proximity to a surface. We assume that the tip is rigid in comparison with the soft sample, so that the interaction force does not cause any deformation of the tip. At any given point x, y in the scan, the vertical position if the tip $z(t)$ and that of the surface $z_s(t)$ may be moving in the inertial reference frame in which the bulk of the sample is at rest. We treat the surface forces with a linear approximation by introducing a coordinate $d_s = z_s - z_0$, which is an effective deflection of the surface from its equilibrium position (see fig. 1 of main paper). Let us first consider a model that includes the inertia associated with the moving surface.

$$\begin{aligned} \frac{1}{\omega_0^2}\ddot{d} + \frac{1}{\omega_0 Q}\dot{d} + d &= \frac{1}{k}F_{\mathrm{TS}}(s,\dot{s}) + \frac{1}{k}F_{\mathrm{D}}(t)\,, && \text{(S10)} \\ \frac{1}{\omega_s^2}\ddot{d}_s + \frac{\eta_s}{k_s}\dot{d}_s + d_s &= -\frac{1}{k_s}F_{\mathrm{TS}}(s,\dot{s})\,, && \text{(S11)} \end{aligned}$$

Note that positive cantilever deflection d and surface deflection d_s are defined in the same direction, away from the surface. The cantilever forces (Eq. S10) are coupled to the surface forces (Eq. S11) via the nonlinear interaction force $F_{\mathrm{TS}}(s,\dot{s})$ which is a function of their separation $s = z - z_s = (h - z_0) + (d - d_s)$.

In this simplified model both the cantilever and surface are described as simple harmonic oscillators. The cantilever has well-defined eigenmodes and our model gives an excellent description of the cantilever dynamics in the experiment, where motion is confined to a narrow frequency band around the fundamental bending mode. On the other hand, the infinite surface has a continuum of modes which are surface waves of different frequency and wavelength, and this simple model describes only a single surface mode. We may estimate a characteristic frequency of surface oscillation ω_s by considering the dispersion relations for surface waves that might be excited by the periodic driving force $F_{\mathrm{D}}(t)$ acting through the nonlinear interaction $F_{\mathrm{TS}}(s,\dot{s})$.

Figure S1 shows the expected frequency of two types of surface waves for a range of materials, over the region of expected wavelength. We expect the lateral extent of surface deformation to be not too much smaller than or larger than the tip radius, of order 10-20 nm. In this wavelength region the frequency of surface waves is 2 or 3 orders of magnitude larger than the frequency of the driving force, the later being close to the cantilever resonance frequency, 100 kHz to 2 MHz depending on the cantilever used. Thus, the finite response time of the surface that we observe in the experiment cannot be due to the inertia of the displaced surface (i.e. $1/\omega_s$ is too small), and therefore must be the result of its viscosity. We conclude that the surface dynamics is over-damped and we may neglect the first term in the right hand side of Eq.S11, bringing us to the model

$$\begin{aligned} \frac{1}{\omega_0^2}\ddot{d} + \frac{1}{\omega_0 Q}\dot{d} + d &= \frac{1}{k}F_{\mathrm{TS}}(s,\dot{s}) + \frac{1}{k}F_{\mathrm{D}}(t)\,, && \text{(S12)} \\ \frac{\eta_s}{k}\dot{d}_s + \frac{k_s}{k}d_s &= -\frac{1}{k}F_{\mathrm{TS}}(s,\dot{s})\,, && \text{(S13)} \end{aligned}$$

where all forces are now normalized by the cantilever stiffness.

Nevertheless, a strongly nonlinear interaction $F_{\mathrm{TS}}(s,\dot{s})$ may result in frequency components of the force at very high harmonics of the drive frequency,

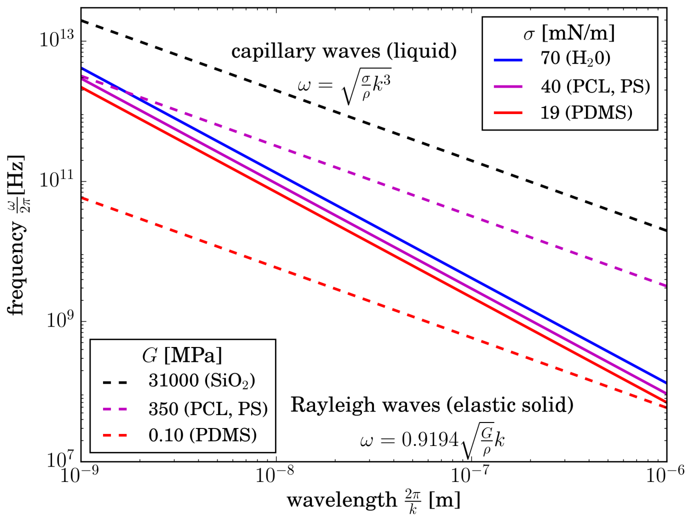

Supplementary Figure S1: Dispersion of surface waves. Frequency vs. wavelength for capilary waves on the surface of a liquid, depending on the density ρ and surface energy (surface tension) σ, and for Rayleigh waves on the surface of an elastic solid, depending on the density and shear modulus G. Plots are shown for approximate values of the materials indicated.

which could excite surface waves. If the surface waves do not reflect from a boundary they will appear to the cantilever as additional radiation damping. An in-homogeneous surface could exhibit localized surface modes, or standing-wave surface oscillations, but to our knowledge no evidence of such surface oscillations has been shown with dynamic AFM experiments.

Simulations

The system is driven by an oscillatory force with two drive tones

$$F_{\mathrm{D}} = \frac{k}{Q}\left(d_1 \cos\omega_1 t + d_2 \cos\omega_2 t\right) . \tag{S14}$$

where d_1 and d_2 are the free amplitudes of the oscillation when the cantilever is driven without the tip-surface interaction. The drive frequencies $\omega_{1,2}$ are chosen such that they satisfy

$$\omega_{1,2} = 2\pi m_{1,2}\Delta f \,, \tag{S15}$$

$$\Delta f = \frac{f_s}{n} \,, \tag{S16}$$

where n, $m_{1,2}$ are integers and f_s is the sampling frequency. We numerically integrate the system using CVODE [11], where the disconunity at $s = 0$ is properly treated using discrete event detection.

The integrator gives output at discrete time steps $t_n = n\Delta t = n/f_s$. Taking the discrete Fourier transform of the motion we obtain the cantilever spectrum,

$$\hat{d}_k(k\Delta\omega) = DFT[d_n(n\Delta t)] \tag{S17}$$

including all intermodulation products of the two drive frequencies. Due to the large quality factor of the cantilever resonance Q, response in a narrow band around the resonance frequency dominates the cantilever motion. Taking only this response, we determine the amplitude dependent force quadratures [1].

Additional Results

Figure S2 displays analysis of a blend of polystyerene (PS) and polydimethylsiloxane (PDMS). The AFM height image $h(x, y)$ is shown for several different feedback set-point values, which was changed during the scan. The feedback adjusts h to keep the response amplitude at one of the two drive tones at a set-point value $S = |\hat{d}(\omega_1)|/|\hat{d}_{\mathrm{free}}(\omega_1)|$. Figure S2a and S2b shows the conservative and dissipative force quadratures $F_I(A)$ and $F_Q(A)$ respectively, measured at the pixels marked with an $\times$ in the corresponding color. The double-curves show both increasing and decreasing oscillation amplitude.

The overall surface height, and the height difference between the two visible domains, depends strongly on the set-point. At lower S both F_I and F_Q are non-zero down to the lowest oscillation amplitude A (yellow and green curves in figs. S2a and S2b). For $S < 0.7$ the tip is always interacting with the surface, experiencing a dominantly repulsive force ($F_I < 0$) that is more viscous than elastic. We conclude that the tip oscillates in continuous contact with a very soft, liquid-like PDMS surface layer. At $S = 0.9$ the tip begins to oscillate in and out of contact with this liquid-like layer, and a characteristic hysteresis in both $F_I(A)$ and $F_Q(A)$ is observed. The shape of these curves, with a positive F_I that is nearly independent of amplitude, has been observed in many experiments on soft, liquid-like surfaces.

Figures S3 and S4 display the analysis of a blend of Polystyrene (PS) and Polyolefin Elastomer (ethylene-octene copolymer, LDPE), spin-cast onto a silicon substrate (Bruker, HarmoniX test sample). This sample has faster relaxation time than the other samples, and hysteresis in the $F_I(A)$ and $F_Q(A)$ curves is not observed with AFM cantilevers having resonance frequencies of only 300 kHz. The measurements shown here used a shorter, stiffer cantilever (150 N/m) with a much higher resonance frequency (f_0 =1.9 MHz). Good agreement between simulation and experiment can be found by adjusting the model parameters, shown in Table S1. Note that on the LDPE region the apparent DMT modulus E and adhesion force (depth of force minimum) both decrease slightly toward the center of the LDPE region. These observations point to difficulties in applying the DMT model for the interaction $F_{\mathrm{con}}(s)$, as

Color	surface stiffness	surface damping	interaction damping	Reduced modulus	Adhesion Force	working distance
PDMS (fig.S2)	k_s [N/m]	η_s [mg/s]	η_i [mg/s]	E^* [MPa]	$F_{\min}$[nN]	$h - z_0$[nm]
red	0.026	.071	.028	0.6	1.3	28.0
cyan	0.026	.071	.028	0.6	1.3	13.0
green	0.026	.071	.028	0.6	1.3	10.0
yellow	0.026	.071	.028	0.6	1.3	-50.0
LDPE (fig.S3)	k_s [N/m]	η_s [mg/s]	η_i [mg/s]	E [MPa]	F_{min}[nN]	$h - z_0$ [nm]
red	0.350	18	0.14	200.0	6.0	11.5
cyan	0.350	18	0.14	180.0	5.5	10.5
green	0.350	18	0.14	160.0	5.0	9.5
yellow	0.350	18	0.14	140.0	4.5	8.5
PS (fig.S4)	k_s [N/m]	η_s [mg/s]	η_i [mg/s]	E [MPa]	F_{min}[nN]	$h - z_0$ [nm]
red	1.500	6.3	0.25	2000.0	9.0	14.0
cyan	1.500	6.3	0.25	2000.0	9.0	12.5
green	1.500	6.3	0.25	2000.0	9.0	11.0
yellow	1.500	6.3	0.25	2000.0	9.0	9.5

Table S1: The model parameter values used for the simulated curves in figs. S2, S3 and S4). The DMT model contains two parameters that were fixed for the simulation: the inter-atomic spacing a_0 =0.3 nm and the tip radius R =10nm. The cantilever eigenmode parameters were set to the values measured during calibration and the drive frequencies were those used in the experiments. For LDPE and PS: $k = 150.$ N/m , $Q = 693.$, $f_0 = 1.904$ MHz and drive frequencies $f_1 = 1.9025$ MHz, $f_2 = 1.9050$ MHz. For PDMS: $k = 28.8$ N/m, $Q = 428$, $f_0 = 324.01$ kHz and drive frequencies $f_1 = 323.75$ kHz, $f_2 = 324.25$ kHz. Both experimental and simulated curves $F_I(A)$ and $F_Q(A)$ were derived from analysis of 30 intermodulation products near resonance.

well as the simplification of treating the surface forces as linear functions of a single degree of freedom d_s and its associated velocity $\dot{d}_s$. Nevertheless, we see how this model captures the basic physics of the interaction and dynamics of the surface and nicely reproduces the hysteresis in the force quadrature curves.

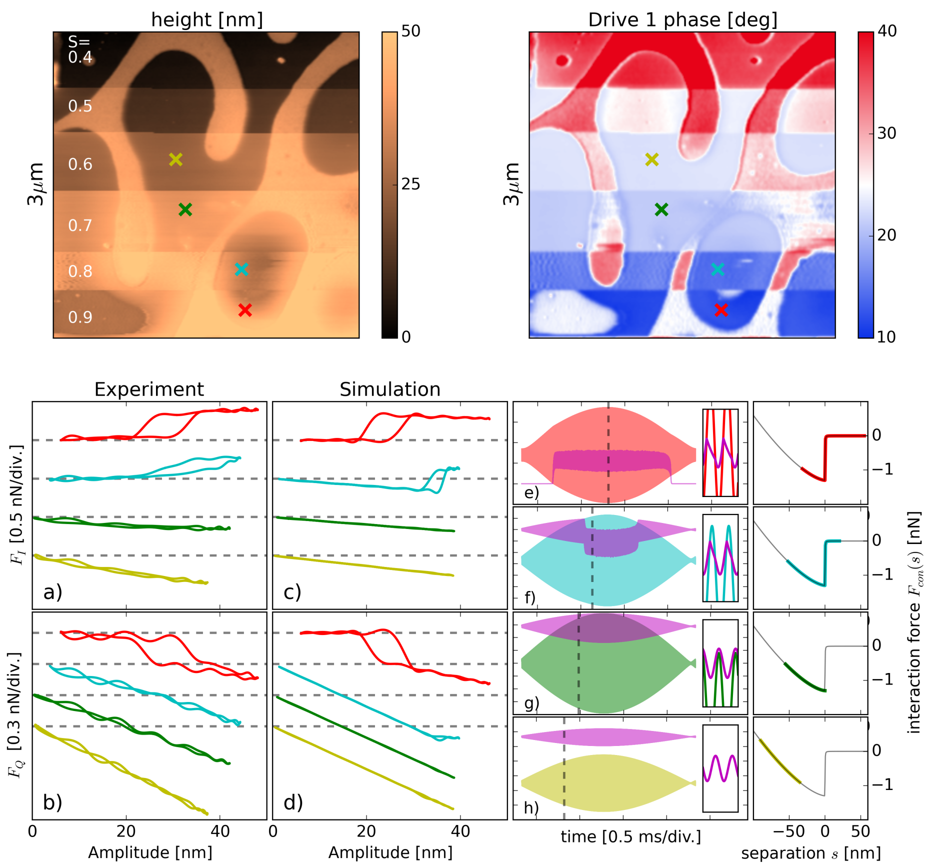

Supplementary Figure S2: The height image and the phase image at the first drive frequency of ImAFM, for a blend of PS and PDMS measured at different feedback set-points heights, S. a) and b) show experimental curves $F_I(A)$ and $F_Q(A)$ at 4 pixels marked in the images with an $\times$ in the corresponding color. Curves are offset and dashed lines indicates zero force. c) and d) are simulated $F_I(A)$ and $F_Q(A)$. e)-h) show the simulated cantilever motion (corresponding color) and surface deflection (magenta) in a the time window $1/\Delta f$. The zoomed insets show individual oscillation cycles at the time marked by the vertical dashed line (all insets have the same vertical scale spanning 60 nm). The right-most column of plots shows the interaction force $F_{\rm con}(s)$ experienced during a simulated time window. The parameters used in the simulations are given in Table S1

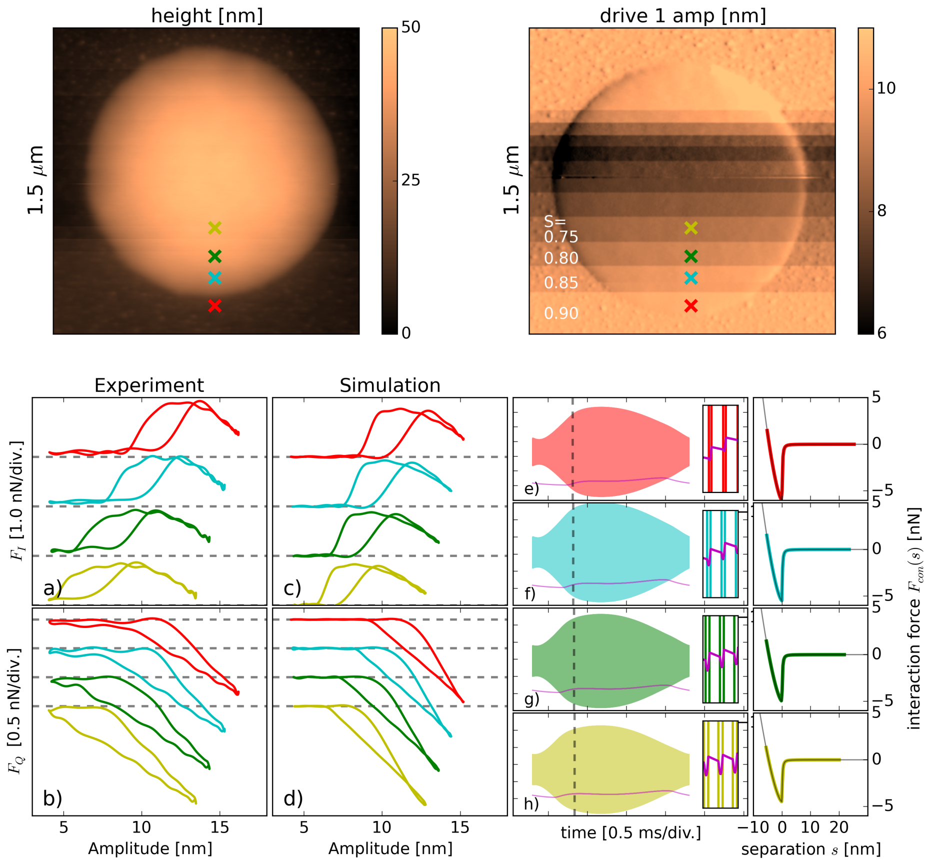

Supplementary Figure S3: Images of the height and the response amplitude at the first drive frequency, where the latter is used for surface tracking feedback. The sample is a blend of PS and LDPE and the feedback set-point S was changed during the scan, giving rise to the banded image. a) and b) show experimental curves $F_I(A)$ and $F_Q(A)$ at 4 pixels in the LDPE region marked in the images with an $\times$ in the corresponding color. Curves are offset vertically and dashed lines indicate zero force. c) and d) are simulated $F_I(A)$ and $F_Q(A)$. e)-h) show the simulated cantilever motion (corresponding color) and surface deflection (magenta) in a time window $1/\Delta f$. The zoomed insets show individual oscillation cycles at the time marked by the vertical dashed line (all insets have the same vertical scale spanning 0.2 nm). The right-most column of plots shows the interaction force $F_{\rm con}(s)$ experienced during a simulated time window. The parameters used in the simulations are given in Table S1

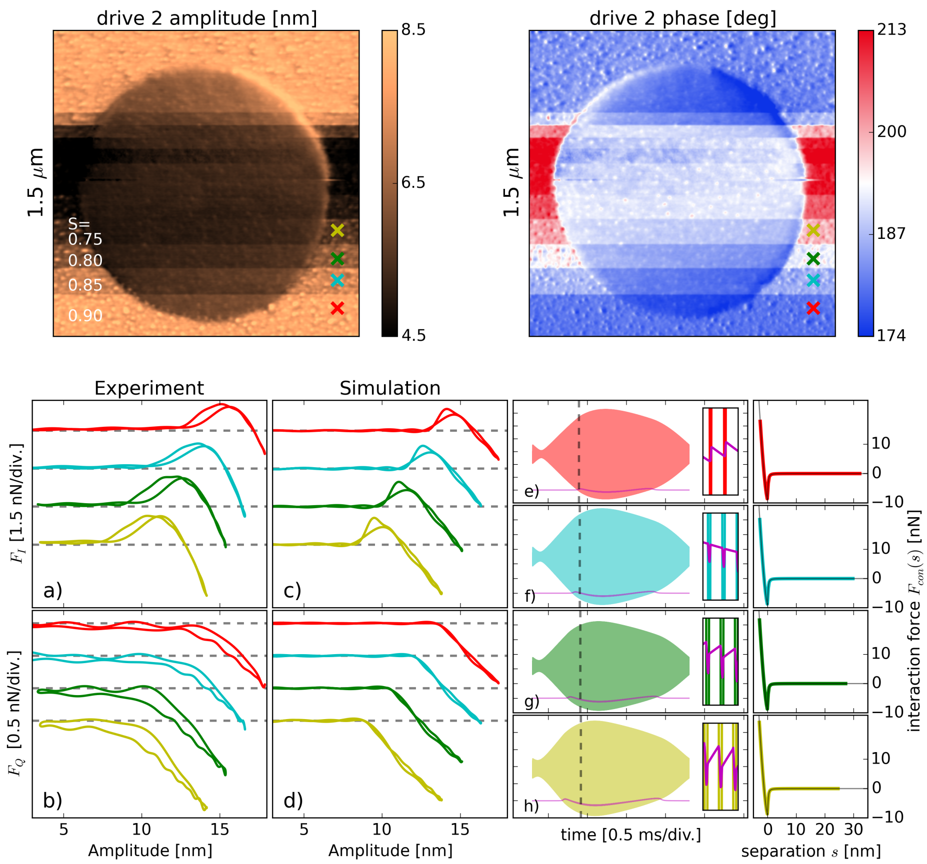

Supplementary Figure S4: The amplitude and phase image at the second drive frequency for the same scan as fig. S3. a) and b) show experimental curves $F_I(A)$ and $F_Q(A)$ at 4 pixels in the PS region marked in the images with an $\times$ in the corresponding color. Curves are offset vertically and dashed lines indicate zero force. c) and d) are simulated $F_I(A)$ and $F_Q(A)$ curves. e)-h) show the simulated cantilever motion (corresponding color) and surface deflection (magenta) in a the time window $1/\Delta f$. The zoomed insets show individual oscillation cycles at the time marked by the vertical dashed line (all insets have the same vertical scale spanning 0.4 nm). The right-most column of plots shows the interaction force $F_{\text{con}}(s)$ experienced during a simulated time window. The parameters used in the simulations are given in Table S1

References

[1] Daniel Platz, Daniel Forchheimer, Erik A. Tholén, and David B. Haviland. Interaction imaging with amplitude-dependence force spectroscopy. *Nat Commun*, 4:1360, 01 2013.

[2] D. Platz, E. A. Tholen, D. Pesen, and D. B. Haviland. Intermodulation atomic force microscopy. *Appl. Phys. Lett.*, 92:153106–1, 2008.

[3] E. A. Tholén, D. Platz, D. Forchheimer, M. O. Tholén, C. Hutter, and D. B. Haviland. The intermodulation lockin analyzer. *Review of Scientific Instruments*, 82:026109, 2011. arXiv:1008.2722v1.

[4] J. E. Sader. Frequency response of cantilever beams immersed in viscous fluids with applications to atomic force microscopy. *Journal of Applied Physics*, 84:64 – 76, 1998.

[5] M. J. Higgins, R. Proksch, J. E. Sader, M. Polcik, S. Mc. Endoo, J. P. Cleveland, and S. P. Jarvis. Noninvasive determination of optical lever sensitivity in atomic force microscopy. *Review of Scientific Instruments*, 77:013701, 2006.

[6] John E Sader, Julian A. Sanelli, Brian D. Adamson, Jason P. Monty, Xingzhan Wei, Simon A. Crawford, James R. Friend, Ivan Marusic, Paul Mulvaney, and Evan J. Bieske. Spring constant calibration of atomic force microscope cantilevers of arbitrary shape. *Review of Scientific Instruments*, 83(10):103705, 2012.

[7] Daniel Platz, Daniel Forchheimer, Erik A. Tholén, and David B. Haviland. Interpreting motion and force for narrow-band intermodulation atomic force microscopy. *Beilstein Journal of Nanotechnology*, 4:45–56, 2013.

[8] Daniel Platz. *Reconstructing force from harmonic motion*. PhD thesis, The Royal Institute of Technology (KTH), 2013.

[9] Daniel Forchheimer. *Imaging materials with intermodulation AFM*. PhD thesis, The Royal Institute of Technology (KTH), 2015.

[10] Hendrik Hölscher, Daniel Ebeling, Jan-Erik Schmutz, Marcus M Schäefer, and Boris Anczykowski. Dynamic force microscopy and spectroscopy using the frequency-modulation technique in air and liquids. In *Scanning Probe Microscopy in Nanoscience and Nanotechnology*, pages 3–21. Springer, 2010.

[11] A. C. Hindmarsh, P. N. Brown, K. E. Grant, S. L. Lee, R. Serban, D. E. Shumaker, and C. S. Woodward ACM. Sundials: Suite of nonlinear and differential/algebraic equation solvers. *Transactions on Mathematical Software*, 31:363–396, 2005.